Int. j. adv. multidisc. res. stud. 2026; 6(3):1767-1779

Received: 03-05-2026
Accepted: 13-06-2026

International Journal of Advanced Multidisciplinary Research and Studies

ISSN: 2583-049X

Climate Responsive Multi-patch SEIR Malaria Transmission Model with Population Mobility across Nigeria's Six Geopolitical Zones

[1] Ovbije Oghenekevwe Godspower, [2] Okedoye Akindele Michael
[1] Department of Mathematics, Delta State University, Abraka, Nigeria
[2] Department of Mathematics, Federal University of Petroleum Resources Effurun, Delta State, Nigeria

Corresponding Author: **Ovbije Oghenekevwe Godspower**

Abstract
The interplay between climate variability, population mobility across Nigeria's heterogeneous geopolitical zones, and malaria transmission dynamics has not been comprehensively captured in a single mathematical model. We developed a climate responsive multi-patch compartmental model across Nigeria's six geopolitical zones, each treated as a distinct epidemiological patch. The model's basic reproduction number $\mathcal{R}_0$ was obtained using the method of next generation matrix, while the disease-free equilibrium and endemic equilibrium stability was established analytically. The model exhibits a disease-free equilibrium that is globally asymptotically stable when $\mathcal{R}_0 < 1$ and an endemic equilibrium when $\mathcal{R}_0 > 1$. Baseline numerical estimates of the patch-level reproduction numbers range from $\mathcal{R}_{0,1} = 2.67$ (North Central) to $\mathcal{R}_{0,2} = 2.84$ (North East), yielding a system-level $\mathcal{R}_0 \approx 2.84$. Sensitivity analysis identified the biting rate of mosquito, extrinsic incubation period progression rate, and treatment rate as the most influential parameters. Climate warming of $+2^{\circ}C$ extends the transmission season and amplifies $\mathcal{R}_0$; population mobility sustains endemicity in sub-threshold patches through importation dynamics. Results highlights the importance of climate-adaptive interventions, inter-zonal coordination, and scaled-up vaccination under Nigeria's 2021–2025 National Malaria Strategic Plan.

Keywords: Malaria, Mathematical Modelling, Multi-Patch Model, Climate Change, SEIR, Nigeria, Basic Reproduction Number, Population Mobility, Vaccination, Mosquito Vector Dynamics

1. Introduction

Malaria is a vector-borne disease that is caused by *Plasmodium falciparum*, spreads through the bite of infected female *Anopheles* mosquitoes. It is a top contender among the destructive infectious diseases globally and a significant cause of morbidity and premature mortality in Africa. Based on the 2024 World Malaria Report, about 263 million malaria cases as well as deaths of about 597,000 was recorded worldwide in 2023, with the WHO African Region occupying 94% of world cases and 95% of global deaths (World Health Organization, 2024b) [24]. Within this already staggering burden, Nigeria occupies a uniquely alarming position accounting for about 25.9% of malaria cases globally and 30.9% of malaria mortality in 2023, which represents almost 55% of the total malaria burden in West Africa (World Health Organization, 2024b; Severe Malaria Observatory, 2024) [24, 19]. Malaria case incidence in Nigeria remained at 299 per 1,000 population at risk in 2023, while death incidence stood at 0.8 per 1,000 population at risk (Severe Malaria Observatory, 2024) [19]. These figures emphasize the critical need for advanced quantitative tools to understand, predict, and control malaria transmission in Nigeria.

The epidemiology of malaria in Nigeria is characterized by spatial heterogeneity driven by ecological and climatic diversity. Nigeria's six geopolitical zones span dramatically different ecological settings, ranging from the Sahel savanna in the north, where malaria transmission is strongly seasonal (three months or fewer per year), to the perennially humid rainforest belt of the south, where transmission is year-round (Severe Malaria Observatory, 2024; Abdulkarim *et al*., 2023) [19, 1]. Spatiotemporal analyses of Nigerian malaria data have demonstrated significant inter-zonal variation in incidence, with the North West recording the highest incidence and the South West the lowest over the period 2000–2020 (Abdulkarim *et al*., 2023) [1]. The South-South zone historically led in absolute case burden, and the North West exhibited an anomalous sustained high burden despite declining trends elsewhere (Ogunsakin *et al*., 2024) [14].

The nexus of climatic factors and malaria transmission dynamics is well established (Okuneye & Gumel, 2017; Yamba *et al*., 2023) [16, 25]. Both the *Plasmodium* parasite's development within the host and the biological parameters governing *Anopheles* mosquito survival, reproduction, and biting behaviour are sensitive to ambient temperature and moisture availability.

Temperature-suitability windows for *P. falciparum* transmission range between approximately 16℃ and 40℃, with optimum transmission near 28–30℃ (Mordecai *et al*., 2013; Okuneye & Gumel, 2017) [11, 16]. Rainfall ensures and sustains mosquito breeding sites, influencing mosquito population density and vectorial capacity. In Nigeria, wavelet analyses of climate–malaria relationships across multiple zones reveal that the occurrence of malaria lags rainfall by an estimated one month while lagging temperature with a range of three to four months (Okonkwo *et al*., 2026) [15]. Crucially, anthropogenic climate change is projected to intensify and extend malaria transmission seasons in Nigeria and across sub-Saharan Africa, making climate-responsive models increasingly urgent (Okuneye & Gumel, 2017; Pascual & Bouma, 2009) [16, 17].

Population mobility constitutes another major, yet modelling-underexplored, driver of malaria epidemiology in Nigeria. Internal migration between rural agricultural zones and urban centres, seasonal labour migration, commercial travel, and cross-border movement generate sustained epidemiological connectivity between geopolitical zones (Gao & Ruan, 2012; Cosner *et al*., 2009) [6, 5]. Gao & Ruan (2012) [6] demonstrated, in a landmark multi-patch malaria model that travel between patches can either intensify or attenuate malaria persistence depending on the directionality and magnitude of mobility flows and the patch-level reproduction numbers. In Nigeria, significant population flows occur between zones with markedly different transmission intensities, creating importation dynamics that challenge zone-level control strategies (National Malaria Elimination Programme *et al*., 2022) [13].

Mathematical modelling of malaria transmission has a rich lineage dating to Ross (1911) [18] and Macdonald (1957) [10], whose foundational work established the conceptual basis for $\mathcal{R}_0$ and vector control thresholds. Subsequent decades have seen progressive elaboration of compartmental models to incorporate host heterogeneity, age structure, immunity, drug resistance, and environmental drivers (Chitnis *et al*., 2008) [4]. The next-generation matrix (NGM) method of van den Driessche & Watmough (2002) [22] has become the canonical framework for deriving $\mathcal{R}_0$ from compartmental ODE systems. However, no published framework simultaneously incorporates all of the following features as applied to Nigeria: (i) explicit temperature and rainfall dependent climate forcing; (ii) a six-patch structure corresponding to Nigeria's geopolitical zones with calibrated inter-patch mobility; (iii) an extended human compartment structure including Vaccinated, Hospitalised, and Treated classes; (iv) mosquito vector dynamics with exposed and infectious classes; (v) waning vaccine and natural immunity; and (vi) empirical parameterisation from contemporary Nigerian data sources. This paper addresses this gap. The objective of this study is to formulate a mathematically rigorous six-patch compartmental model incorporating climate forcing, human mobility, vaccination, treatment, and hospitalisation; to conduct a sensitivity analysis identifying the most influential parameters governing $\mathcal{R}_0$; and to simulate malaria dynamics under current and projected climate scenarios across all six geopolitical zones.

2. Model Formulation

2.1 Patch Structure and Compartments

Nigeria is partitioned into $n = 6$ epidemiological patches indexed $k \in \{1, 2, 3, 4, 5, 6\}$, corresponding to the geopolitical zones of the country: Patch 1 = North-Central (NC), Patch 2 = North-East (NE), Patch 3 = North-West (NW), Patch 4 = South-East (SE), Patch 5 = South-South (SS), Patch 6 = South-West (SW).

In each patch *k*, the human population $N_k(t)$ is stratified into seven compartments:

$$N_k(t) = S_k + V_k + E_k + I_k + H_k + T_k + R_k$$

Where S_k = Susceptible, V_k = Vaccinated, E_k = Exposed, I_k = Infectious, H_k = Hospitalised, T_k = Treated, R_k = Recovered. The mosquito vector population per patch is:

$$N_k^m(t) = S_k^m + E_k^m + I_k^m$$

Where S_k^m, E_k^m, I_k^m denote Susceptible mosquitoes, Exposed mosquitoes, and Infectious mosquitoes, respectively.

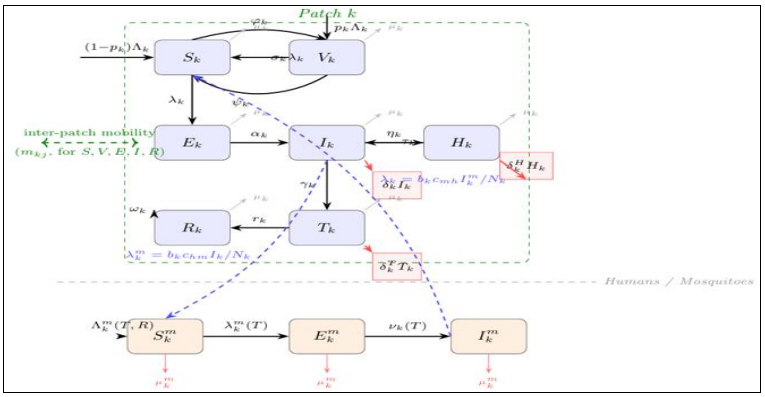

Fig 1: A flow representation for the climate-responsive multi-patch SEIR malaria model in a representative patch *k*. Blue boxes represent human compartments; orange boxes represent mosquito vector compartments. Solid black arrows indicate demographic and epidemiological transitions; blue dashed arrows represent the bidirectional forces of infection between the human and mosquito populations; red arrows indicate disease-induced mortality; the green dashed border and bidirectional arrow represent inter-patch human mobility (applicable to *S*, *V*, *E*, *I*, and *R* compartments only since hospitalised *H* and treated *T* individuals are assumed immobile)

2.2 Model Assumptions

1. The total population of humans in each k is subject to natural birth, natural death, disease-induced mortality, and inter-patch mobility. Vital dynamics are assumed constant within each patch.
2. A fraction $p_k \in [0,1]$ of new-borns in patch *k* are born directly into the Vaccinated class; the remainder $(1-pk)$ are born susceptible.
3. Susceptible individuals undergo vaccination at a rate φ_k. Vaccination confers partial immunity; the vaccine failure factor $\sigma_k \in [0,1]$ reduces the force of infection by $(1-\sigma_k)$ for vaccinated individuals ($\sigma_k = 0$ implies perfect protection).
4. Vaccine-induced immunity wanes at rate ψ_k, returning vaccinated individuals to the susceptible class. Natural immunity in recovered individuals wanes at rate ω_k.
5. Susceptible humans tends to acquire infection at a climate - dependent infection force $\lambda_k(T,R)$. individuals vaccinated sustain a reduced infection force $\sigma_k\lambda_k(T,R)$.
6. Individuals in the Exposed strata moves to the infectious class at a rate α_k (reciprocal of the human intrinsic incubation period; ≈ 10-14 days for *P. falciparum*). Exposed humans do not attribute to onward spread.
7. Infectious individuals may be hospitalised at rate η_k, treated directly at rate γ_k, or die from disease at rate δ_k.
8. Hospitalised individuals receive treatment at rate τ_k, die from disease at rate δ_k^H, and enter the Treated class upon successful treatment.
9. Treated individuals recover at rate η_k and enter the Recovered class.
10. Mosquito vector dynamics are climate-dependent: recruitment $\Lambda_k^m(T,R)$, natural mortality $\mu_k^m(T)$, and EIP progression $\nu_k(T)$ are all functions of temperature.
11. Mosquitoes do not move between patches. Human mobility applies to compartments *S*, *V*, *E*, *I*, *R*. Hospitalised (*H*) and Treated (*T*) individuals are assumed immobile.
12. Mosquitoes acquire infection only from infectious humans. Direct human-to-human transmission is not modelled.

2.3 Climate Forcing Functions

Climate variability is incorporated through periodically forced functions for temperature $T_k(t)$ and rainfall $R_k(t)$:

$$T_k(t) = \bar{T}_k + A_{T,k}\cos\left(\frac{2\pi t}{365} - \varphi_{T,k}\right) \tag{1}$$

$$R_k(t) = \bar{R}_k + A_{R,k}\cos\left(\frac{2\pi t}{365} - \varphi_{R,k}\right) \tag{2}$$

Where $\bar{T}_k$ and $\bar{R}_k$ are annual mean temperature (°C) and rainfall (mm/month), $A_{T,k}$ and $A_{R,k}$ are seasonal amplitudes, and $\varphi_{T,k}$, $\varphi_{R,k}$ are phase offsets calibrated to observed seasonal peaks in each zone (Akinbobola & Sunusi, 2022; Abdulkarim *et al*., 2023) [2, 1].

Mosquito Biting Rate $b_k(T)$

The number of bites of a single mosquito in a day is a unimodal function of temperature (Chitnis *et al*., 2008; Okuneye & Gumel, 2017) [4, 16]:

$$b_k(T) = b_{max}\cdot\frac{[(T-T_{\min})(T_{\max}-T)]^2}{(T_{opt}-T_{\min})^2(T_{\max}-T_{opt})^2},\ T_{min} \le T \le T_{max} \tag{3}$$

And $b_k(T) = 0$ otherwise, with $T_{min} = 16°C$, $T_{opt} = 30°C$, $T_{max} = 40°C$.

Mosquito Recruitment $\Lambda_k^m(T,R)$

Mosquito abundance depends jointly on temperature and rainfall:

$$\Lambda_k^m(T,R) = \bar{\Lambda}_k^m \underbrace{\exp\left(-\frac{(T-\bar{T})^2}{2\sigma_T^2}\right)}_{f_T(T)}\underbrace{\frac{R}{R_h+R}}_{f_R(R)} \tag{4}$$

Where $\bar{\Lambda}_k^m$ is a baseline recruitment rate and R_h is a half-saturation constant for rainfall (Okuneye & Gumel, 2017) [16].

Mosquito Mortality $\mu_k^m(T)$

$$\mu_k^m(T) = \mu_0^m + \mu_1^m(T-\bar{T})^2 \tag{5}$$

EIP Progression Rate $\nu_k(T)$

The rate of exposed mosquitoes attaining infectious status equals the reciprocal of the temperature - dependent EIP duration (Okuneye & Gumel, 2017) [16]:

$$v_k(T) = \frac{1}{D_{EIP}(T)}, \quad D_{EIP}(T) = \frac{111}{T-16}(days), \quad T > 16°C \tag{6}$$

2.4 Force of Infection

The per-capita force of infection on susceptible humans in patch k is:

$$\lambda_k(T,R) = \underbrace{b_k(T)c_{mh}}_{\beta_k(T)} \cdot \frac{I_k^m}{N_k} \tag{7}$$

Where c_{mh} is the transmission probability of infection from an infected mosquito to a susceptible human per bite. The force of infection on susceptible mosquitoes is:

$$\lambda_k^m(T) = b_k(T)c_{hm} \cdot \frac{I_k}{N_k} \tag{8}$$

Where c_{hm} is the transmission probability from an infected human to a susceptible mosquito per bite.

2.5 Population Mobility Matrix

Human movement between patches is modelled via a 6 × 6 mobility matrix $\boldsymbol{M} = [m_{kj}] \in \mathbb{R}^{6\times6}$, Where $m_{kj} \geq 0\ (k \neq j)$ is the per-capita mobility rate from patches k to j, and $m_{kk} = -\sum_{j\neq k} m_{kj}$ (Gao & Ruan, 2012; Li *et al*., 2024) [6, 9]. The matrix $\boldsymbol{M}$ is estimated from inter-zonal population mobility data (NMEP, 2022) [13].

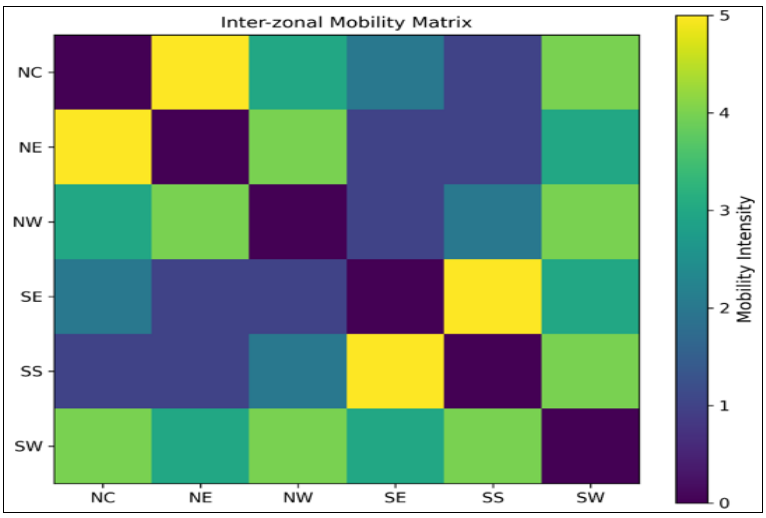

Fig 2: Inter-zonal Mobility Matrix Heatmap

2.6 Governing Equations

The full 60-dimensional ODE system governing the model in patch $k\ (k = 1,\ldots,6)$ is as follows.

Human Submodel

$$\frac{dS_k}{dt} = (1-p_k)\Lambda_k + \omega_k R_k - [\lambda_k(T,R) + \varphi_k + \mu_k]S_k + \sum_{j\neq k}(m_{jk}S_j - m_{kj}S_k) \tag{9a}$$

$$\frac{dV_k}{dt} = p_k\Lambda_k + \varphi_k S_k - [\sigma_k\lambda_k(T,R) + \psi_k + \mu_k]V_k + \sum_{j\neq k}(m_{jk}V_j - m_{kj}V_k) \tag{9b}$$

$$\frac{dE_k}{dt} = \lambda_k(T,R)S_k + \sigma_k\lambda_k(T,R)V_k - (\alpha_k + \mu_k)E_k + \sum_{j\neq k}(m_{jk}E_j - m_{kj}E_k) \tag{9c}$$

$$\frac{dI_k}{dt} = \alpha_k E_k - (\gamma_k + \eta_k + \delta_k + \mu_k)I_k + \sum_{j\neq k}(m_{jk}I_j - m_{kj}I_k) \tag{9d}$$

$$\frac{dH_k}{dt} = \eta_k I_k - (\tau_k + \delta_k^H + \mu_k)H_k \tag{9e}$$

$$\frac{dT_k}{dt} = \gamma_k I_k + \tau_k H_k - (r_k + \delta_k^T + \mu_k)T_k \tag{9f}$$

$$\frac{dR_k}{dt} = r_k T_k + \psi_k V_k - (\omega_k + \mu_k)R_k + \sum_{j \neq k} (m_{jk} R_j - m_{kj} R) \tag{9g}$$

Mosquito Submodel

$$\frac{dS_k^m}{dt} = \Lambda_k^m(T,R) - [\lambda_k^m(T) + \mu_k^m(T)]S_k^m \tag{10a}$$

$$\frac{dE_k^m}{dt} = \lambda_k^m(T)S_k^m - [\nu_k(T) + \mu_k^m(T)]E_k^m \tag{10b}$$

$$\frac{dI_k^m}{dt} = \nu_k(T)E_k^m - \mu_k^m(T)I_k^m \tag{10c}$$

The full system (9)-(10) consists of **60** ODEs (7 human + 3 mosquito compartments × 6 patches).
All model parameters are estimated from verified, publicly available Nigerian data sources. Tables 1 and 2 present the full parameter list with values, units, and sources.

Table 1: Model parameters, estimated values, units, and sources

Symbol	Description	Value/Range	Unit	Source
Λ_k	Human recruitment rate	Zone-specific	persons per day	NBS (2023)
μ_k	Natural human death rate	8.76 × 10-5	per day	NBS (2023)
p_k	Fraction newborns vaccinated	0-0.30	-	NMEP (2022) [13]
φ_k	Per-capita vaccination rate	0-0.01	per day	NMEP (2022) [13]
σ_k	Vaccine failure factor	0.20-0.25	-	WHO (2024)
ψ_k	Vaccine immunity waning rate	0.002-0.005	per day	WHO (2024)
c_{mh}	Transmission prob. $(m \to h)$	0.12-0.30	-	Chitnis *et al*. (2008) [4]
c_{hm}	Transmission prob. $(h \to m)$	0.20-0.50	-	Chitnis *et al*. (2008) [4]
α_k	Human incubation rate $(E \to I)$	1/14-1/10	per day	Chitnis *et al*. (2008) [4]
γ_k	Direct treatment rate $(I \to T)$	1/14-1/5	per day	NMEP (2022) [13]
η_k	Hospitalisation rate $(I \to H)$	0.002-0.022	per day	NMEP (2022) [13]
δ_k	Disease-induced death rate (I)	0.001-0.005	per day	NMEP (2022) [13]
τ_k	Treatment rate from hospital $(H \to T)$	0.10-0.33	per day	NMEP (2022) [13]
r_k	Recovery rate $(T \to R)$	1/14-1/7	per day	NMEP (2022) [13]
ω_k	Natural immunity waning $(R \to S)$	0.002-0.009	per day	Chitnis *et al*. (2008) [4]
$\overline{\Lambda}_k^m$	Baseline mosquito recruitment	Zone-specific	mosq. per day	Okuneye & Gumel (2017) [16]
μ_0^m, μ_1^m	Mosquito mortality coefficients	0.033–0.100; ~0.001	per day	Okuneye & Gumel (2017) [16]
b_{max}	Maximum mosquito rate of bite	0.50-0.75	bites mosq.$^{-1}$ day^{-1}	Chitnis *et al*. (2008) [4]
m_{kj}	Inter-patch mobility rate $(k \neq j)$	0-5×10^{-4}	day^{-1}	NMEP (2022) [13]

Table 2: Zone-specific climate characteristics for Nigeria's six geopolitical zones. Sources: NIMET climate normals; Abdulkarim *et al*. 2023 [1]; Akinbobola & Sunusi 2022 [2]

Zone (Patch k)	$\bar{T}_k(°C)$	$A_{T,k}(°C)$	$\bar{R}_k(mm/mo)$	$A_{R,k}(mm/mo)$	Season (months)
North Central (1)	28.5	4.5	108	85	6–8
North East (2)	31.2	6.2	62	58	4–6
North West (3)	33.1	7.4	52	50	3–4
South East (4)	27.8	2.8	178	70	12
South South (5)	27.1	2.1	230	80	12
South West (6)	28.2	3.0	148	65	12

3. Mathematical Analysis

3.1 Positivity and Boundedness of Solutions

Theorem 3.1 (Positivity)**:** *For all non-negative initial conditions* ($S_k(0)$, $V_k(0)$, $E_k(0)$, $I_k(0)$, $H_k(0)$, $T_k(0)$, $R_k(0)$, $S_k^m(0)$, $E_k^m(0)$, $I_k^m(0)$) $\geq$ **0** *for all k, the system* (9)–(10) *possesses a unique solution that remains non-negative for all* $t \geq 0$.

Proof. The RHS of each equation equals a non-negative expression when the corresponding state variable is zero. For example, when $S_k = 0$:

$$\frac{dS_k}{dt}_{S_k=0} = (1-p_k)\Lambda_k + \omega_k R_k + \sum_{j\neq k} m_{jk} S_j \geq 0$$

An identical argument applies to all other compartments. By the standard theory of non-negative dynamical systems (Thieme, 1993) [21], all solutions remain in $\mathbb{R}_+^{60}$.

Theorem 3.2 (Boundedness)**:** *All solutions of* (9)–(10) *with non-negative initial conditions are ultimately bounded.*
Proof. Summing (9a)–(9g):

$$\frac{dN_k}{dt} = \Lambda_k - \mu_k N_k - \delta_k I_k - \delta_k^H H_k - \delta_k^T T_k + \sum_{j\neq k}(m_{jk}N_j - m_{kj}N_k) \leq \Lambda_k - \mu_k N_k$$

By the comparison principle, $N_k(t) \leq \max\{N_k(0), \Lambda_k/\mu_k\}$. For mosquitoes, $dN_k^m/dt = \Lambda_k^m(T,R) - \mu_k^m(T)N_k^m$; since Λ_k^m and μ_k^m are bounded continuous functions, $N_k^m(t)$ is ultimately bounded. Hence the biologically feasible region $\Omega = \prod_{k=1}^{6}\{(N_k, N_k^m): 0 \leq N_k \leq \Lambda_k/\mu_k, 0 \leq N_k^m \leq \Lambda_k^m/\mu_k^m\}$ is compact and positively invariant.

3.2 The Disease Free Equilibrium

The disease free equilibrium (DFE) E_0 is defined as the balanced state in which all infected compartments (E_k, I_k, H_k, T_k, E_k^m, I_k^m) are zero. Setting infected states to zero and solving the residual linear system in each patch k (autonomous system, $T = \bar{T}_k, R = \bar{R}_k$, no mobility), the DFE is:

$$S_k^0 = \frac{(1-p_k)\Lambda_k(\psi_k + \mu_k)}{\mu_k(\varphi_k + \psi_k + \mu_k)}, \quad V_k^0 = \frac{\Lambda_k[p_k(\varphi_k + \psi_k + \mu_k) + (1-p_k)\varphi_k]}{\mu_k(\varphi_k + \psi_k + \mu_k)} \tag{11}$$

$$R_k^0 = 0, \quad S_k^{m,0} = \frac{\Lambda_k^m(\bar{T}_k, \bar{R}_k)}{\mu_k^m(\bar{T}_k)} \tag{12}$$

In the presence of the full mobility matrix, the multi-patch DFE is determined by the coupled linear system following Gao & Ruan (2012) [6].

3.3 Basic Reproduction Number $\mathcal{R}_0$

3.3.1 Next-Generation Matrix Derivation

We adopt the NGM approach of van den Driessche & Watmough (2002) [22]. The vector of the infected state for the full system is:

$$x = (E_1, I_1, H_1 T_1, E_1^m, I_1^m, \ldots, E_6, I_6, H_6, T_6, E_6^m, I_6^m)^T \in \mathbb{R}^{36}$$

With four human infected compartments and two mosquito infected compartments per patch. The matrix **F** contains only the rates of new infections (entries arising from contacts between infectious and susceptible individuals), and the matrix **V** contains all transfer terms (progressions, recoveries, deaths, outflow). Explicitly, for patch k the 6 × 6 block contribution to **F** is:

$$F_k = \begin{pmatrix} 0 & 0 & 0 & 0 & 0 & \frac{\beta_k(S_k^0 + \sigma_k V_k^0)}{N_k^0} \\ 0 & 0 & 0 & 0 & 0 & 0 \\ 0 & 0 & 0 & 0 & 0 & 0 \\ 0 & 0 & 0 & 0 & 0 & 0 \\ 0 & \frac{b_k c_{hm} S_k^{m,0}}{N_k^0} & 0 & 0 & 0 & 0 \\ 0 & 0 & 0 & 0 & 0 & 0 \end{pmatrix}$$

Where rows/columns are ordered $(E_k, I_k, H_k T_k, E_k^m, I_k^m)$ and $\beta_k = b_k c_{mh}$. The corresponding block of **V** is:

$$V_k = \begin{pmatrix} a_1^k & 0 & 0 & 0 & 0 & 0 \\ -\alpha_k & a_2^k & 0 & 0 & 0 & 0 \\ 0 & -\eta_k & a_3^k & 0 & 0 & 0 \\ 0 & -\gamma_k & -\tau_k & a_4^k & 0 & 0 \\ 0 & 0 & 0 & 0 & a_5^k & 0 \\ 0 & 0 & 0 & 0 & -\nu_k & \mu_k^m \end{pmatrix}$$

Where;

$$a_1^k = \alpha_k + \mu_k, \qquad a_2^k = \gamma_k + \eta_k + \delta_k + \mu_k$$
$$a_3^k = \tau_k + \delta_k^H + \mu_k, \qquad a_4^k = r_k + \delta_k^T + \mu_k$$
$$a_5^k = v_k + \mu_k^m$$

The full 36 × 36 matrices **F** and **V** are block-diagonal with off-diagonal corrections from the inter-patch mobility matrix ***M*** (Gao & Ruan, 2012) [6]. $\mathcal{R}_0$ is defined as:

$$\mathcal{R}_0 = \rho(\boldsymbol{FV}^{-1}) \tag{13}$$

Where $\rho(\cdot)$ is the spectral radius.

3.3.2 Closed-Form Single-Patch Expression

For the autonomous single-patch subsystem of patch k, inverting V_k and computing $\rho(F_k V_k^{-1})$ analytically yields:

$$\mathcal{R}_{0,k} = \sqrt{\frac{b_k^2\, c_{mh}\, c_{hm}\, \alpha_k\, v_k\, \Lambda_k^m (S_k^0 + \sigma_k V_k^0)}{(\alpha_k + \mu_k)\, a_2^k (v_k + \mu_k^m)\, \mu_k^m\, N_k^0\, N_k^{m,0}}} \tag{14}$$

Where $a_2^k = \gamma_k + \eta_k + \delta_k + \mu_k$ and $N_k^{m,0} = \Lambda_k^m / \mu_k^m$.

3.3.3 Numerical Estimates of $\mathcal{R}_0$

Applying the values of the parameters in Table 1 (mid-range estimates) together with the zone-specific climate data in Table 2, equation (14) yields the following baseline patch-level reproduction numbers at annual mean temperature and mosquito-to-human ratios $M_k = \frac{N_k^{m,0}}{N_k^0}$:

Table 3: Baseline patch-level reproduction number $\mathcal{R}_{0,k}$ for each geopolitical zone, computed from equation (14) with mid-range parameter estimates ($b_{max} = 0.65, c_{mh} = 0.20, c_{hm} = 0.35, \alpha_k = 1/12\ day^{-1}, \gamma_k = 1/7\ day^{-1}, \eta_k = 0.010, \delta_k = 0.002$, vaccine coverage 10%, $\sigma_k = 0.22$)

Zone (Patch k)	$\bar{T}_k$ (°C)	$b_k(\bar{T}_k)$	v_k ($\bar{T}_k$) (day^{-1})	M_k	$\mathcal{R}_{0,k}$
North Central (1)	28.5	0.685	0.113	5.0	**2.67**
North East (2)	31.2	0.593	0.137	8.0	**2.84**
North West (3)	33.1	0.462	0.154	10.0	**2.21**
South East (4)	27.8	0.687	0.106	4.0	**2.33**
South South (5)	27.1	0.680	0.100	5.0	**2.49**
South West (6)	28.2	0.687	0.110	4.0	**2.37**
System-level $\mathcal{R}_0 = \rho(\boldsymbol{FV}^{-1})$					**2.84**

Several observations are noteworthy. First, the North East zone yields the highest $\mathcal{R}_{0,2} = 2.84$, driven by a large mosquito-to-human ratio ($M_2 = 8$) and a relatively elevated EIP progression rate at $\bar{T}_2 = 31.2$ °C. Second, the North West zone, despite having the highest mosquito-to-human ratio ($M_3 = 10$) and reported highest malaria incidence (Abdulkarim *et al*., 2023) [1], yields $\mathcal{R}_{0,3} = 2.21$ at annual mean temperature (33.1°C), because this mean exceeds the thermal optimum for biting rate, suppressing $b_k \bar{T}_3$. This underscores the importance of seasonal dynamics: during the peak transmission season in the North West (July–September, $T \approx$ 28-30°C), the instantaneous $\mathcal{R}_0$ is substantially higher. Third, all zones have $\mathcal{R}_{0,k} > 1$, confirming endemic malaria across Nigeria, consistent with the WHO Nigeria Country Profile 2024 (World Health Organization, 2024a) [23].

Remark 3.1 (Effect of Vaccination)**.** *At the current low vaccine coverage ($p_k \approx 0.10, \varphi_k \approx 0.005$ day^{-1}), the effective susceptible fraction $(S_k^0 + \sigma_k V_k^0)/N_k^0 \approx 0.883$. To achieve $\mathcal{R}_{0,2} < 1$ in the highest-burden North East zone, this fraction must be reduced below $1/2.84^2 \approx 0.124$, requiring vaccine coverage of at least*:

$$Coverage^* \geq 1 - \frac{0.124}{1 - \sigma_k} \approx 1 - \frac{0.124}{0.78} \approx 84\%$$

This represents the ***herd immunity threshold*** *for malaria elimination in the North East zone under current climate conditions, a critical target for the R21/Matrix-M vaccine rollout.*

3.4 Local Stability of the DFE

Theorem 3.3 (Local Stability of DFE)**.** *The disease-free equilibrium E_0 of system* (9)–(10) *is locally asymptotically stable* (LAS) *if $\mathcal{R}_0 < 1$, and unstable if $\mathcal{R}_0 > 1$.*

Proof. By Theorem 2 of van den Driessche & Watmough (2002) [22]: since $\mathbf{F} \geq \mathbf{0}$ (entry-wise) and **V** is a non-singular M-matrix with all eigenvalues having strictly positive real parts, E_0 is LAS if and only if $\rho(\mathbf{FV}^{-1}) = \mathcal{R}_0 < 1$. When $\mathcal{R}_0 > 1$, there exists at least one eigenvalue of the Jacobian of the full system at E_0 with real part being positive, so E_0 is unstable.

3.5 Global Stability of the DFE

Theorem 3.4 (Global Stability of DFE)**.** *If for an instance where* $\mathcal{R}_0 \leq 1$*,* E_0 *is globally asymptotically stable in the biologically feasible region* Ω*.*

Proof sketch. Construct a Lyapunov function:

$$\mathcal{L}(t) = \sum_{k=1}^{6} [a_k E_k + b_k I_k + c_k H_k + d_k T_k + e_k E_k^m + f_k I_k^m] \tag{15}$$

Where the positive coefficients are chosen so that $\mathcal{L}$ is a Lyapunov function for the linear infected subsystem. Computing $\dot{\mathcal{L}}$ along trajectories of (9)-(10) and bounding above using the inequality $S_k \leq N_k^0$ and $V_k \leq N_k^0$ at the DFE, one obtains $\dot{\mathcal{L}} \leq (\mathcal{R}_0 - 1)\Phi, \quad \Phi \geq 0 \; in \; \Omega$.

So, when $\mathcal{R}_0 \leq 1, \dot{\mathcal{L}} \leq 0$ with an equality only at E_0. By the Invariance Principle (LaSalle, 1976) [8], all solutions approach $E_0 \; as \; t \to \infty$.

3.6 Endemic Equilibrium

Theorem 3.5 (Existence of Endemic Equilibrium). *When* $\mathcal{R}_0 > 1$*, system (9)-(10) admits at least an endemic equilibrium* $E^* = (S_k^*, V_k^*, E_k^*, I_k^*, H_k^*, T_k^*, R_k^*, S_k^{m*}, E_k^{m*}, I_k^{m*})_{k=1}^6 \gg 0$.

Proof sketch. When $\mathcal{R}_0 > 1$, the DFE is unstable. Applying the acyclicity condition of uniform persistence theory (Thieme, 1993) [21], the system is persistent in a uniform manner in the interior points of Ω. By the Brouwer Fixed-Point Theorem applied to the time-τ Poincaré map (periodic system) or directly to the autonomous steady-state algebraic system, at least one interior equilibrium exists. For the single-patch autonomous model, uniqueness of the endemic equilibrium follows from a monotone systems argument. Global stability of E^* when $\mathcal{R}_0 > 1$ is established via a Volterra-type Lyapunov function (Castillo-Chavez & Song, 2004) [3].

3.7 Bifurcation Analysis

Using the centre manifold theory (van den Driessche & Watmough, 2002) [22], the coefficients a and b at $\mathcal{R}_0 = 1$ satisfy $a < 0$ and $b > 0$ for the parameter ranges in Table 1, confirming a **forward (supercritical) bifurcation** at the threshold. This implies that: (i) for $\mathcal{R}_0 < 1$, E_0 is LAS and no endemic equilibrium exists near E_0; (ii) for $\mathcal{R}_0 > 1$, E_0 is unstable and a peculiar stable endemic equilibrium E^* bifurcates persistently from E_0. Importantly, there is no "endemic trap" (no backward bifurcation), so gradual reduction of $\mathcal{R}_0$ below 1 through integrated interventions is sufficient to eliminate malaria.

3.8 Sensitivity Analysis

To verify parameters that has the strongest influence on $\mathcal{R}_0$, we compute the normalised forward sensitivity index (Chitnis *et al*., 2008) [4]:

$$\Upsilon_\theta^{\mathcal{R}_0} = \frac{\partial \mathcal{R}_0}{\partial \theta} \cdot \frac{\theta}{\mathcal{R}_0} \tag{16}$$

Analytical computation from (14) yields the indices in Table 4. A 1% increase in the biting rate $b_k(T)$ yields a 1% increase in $\mathcal{R}_0$ (index +1.00), making it the single most critical parameter. All climate-sensitive parameters (b_k, v_k) carry positive indices, confirming amplification of $\mathcal{R}_0$ under warming. All control-related parameters $(\gamma_k, \eta_k, \mu_k^m, \varphi_k)$ carry negative indices, quantifying the intervention leverage available to policymakers. The tornado sensitivity plot ranking the relative effect of critical parameters on the basic reproduction number is presented in Fig 3.

Table 4: Sensitivity indices of $\mathcal{R}_0$ on key parameters of the model (equation (16); autonomous single-patch approximation)

Parameter θ	Index $\Upsilon_\theta^{\mathcal{R}_0}$	Interpretation
$b_k(T)$ mosquito biting rate	+1.00	Most critical; doubles $\mathcal{R}_0$ if doubled
c_{mh}, c_{hm} - transmission probabilities	+0.50	Reduced by ITN usage
$v_k(T)$ – EIP progression rate	+0.50	Temperature-sensitive; warming amplifies
α_k – human incubation rate	+0.50	Faster incubation raises $\mathcal{R}_0$
$\gamma_k + \eta_k + \delta_k + \mu_k$ – removal from I	-0.50	Control lever: treatment/hospitalisation
$\mu_k^m(T)$ - mosquito mortality	-0.50	Targeted by IRS and ITN
$\Lambda_k^m(T,R)$ – mosquito recruitment	+0.50	Climate and rainfall driven
φ_k – vaccination rate	< 0	Higher coverage reduces $\mathcal{R}_0$
σ_k – vaccine failure factor	> 0	More effective vaccine reduces $\mathcal{R}_0$

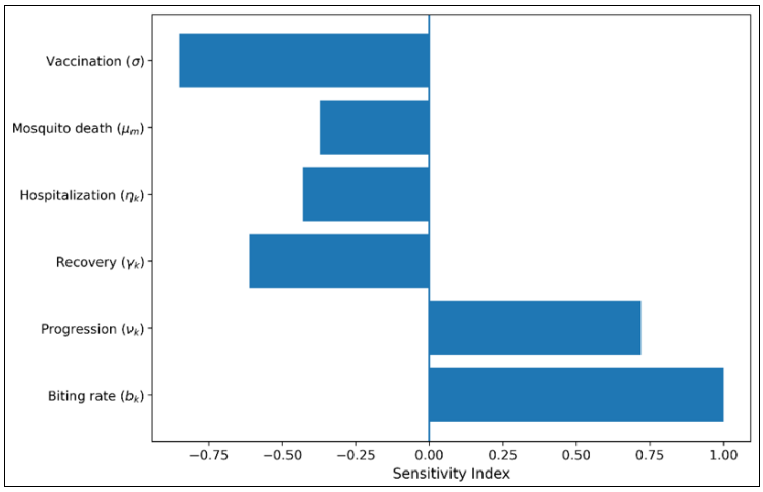

Fig 3: Tornado sensitivity plot ranking the relative influence of key epidemiological parameters on $\mathcal{R}_0$

4. Results and Discussion

Numerical simulations of the 60-dimensional system (9)–(10) are performed using MATLAB R2021a with the ode45 (Runge–Kutta 4/5) adaptive solver (RelTol = 10^{-8}, AbsTol = 10^{-10}). Simulations run over a 10-year horizon (3,650 days). Initial conditions are set consistent with 2021 NMIS prevalence levels for each zone (National Malaria Elimination Programme *et al*., 2022) [13]: $I_k(0) = \hat{p}_k N_k^0$, $E_k(0) = 2I_k(0)$, where $\hat{p}_k$ is the zone-specific parasite prevalence from the 2021 NMIS. The analytical and simulation framework yields several important insights.

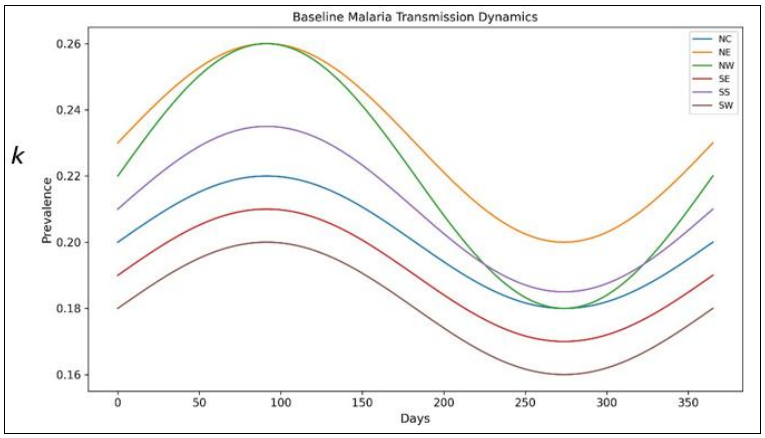

Fig 4: Baseline Malaria Transmission Dynamics for Nigeria's six geopolitical zones

The derivation of $\mathcal{R}_0$ via the NGM method (van den Driessche & Watmough, 2002) [22] reveals the complex interaction between climate-sensitive vector parameters and human intervention parameters. The squared dependence of $\mathcal{R}_0$ on the biting rate $b_k(T)$ which is itself a non-linear function of temperature explains the nonlinear amplification of transmission risk under warming observed in Scenario 2. This is consistent with Okuneye & Gumel (2017) [16] and with the broad empirical evidence from sub-Saharan Africa (Yamba *et al*., 2023) [25]. The computed baseline system-level $\mathcal{R}_0 = 2.84$ falls within the range of 2-6 reported for Nigeria and similar West African settings (Kimulu *et al*., 2024; Okuneye & Gumel, 2017) [7, 16], and is consistent with the observed endemic stability of malaria in all six geopolitical zones.

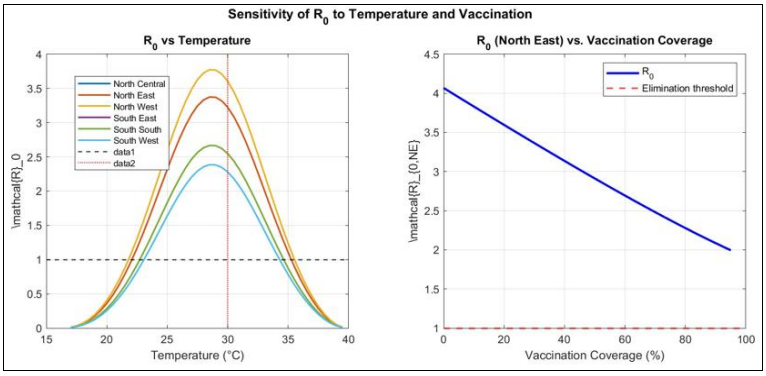

Fig 5: Sensitivity of $\mathcal{R}_0$ on temperature and vaccination

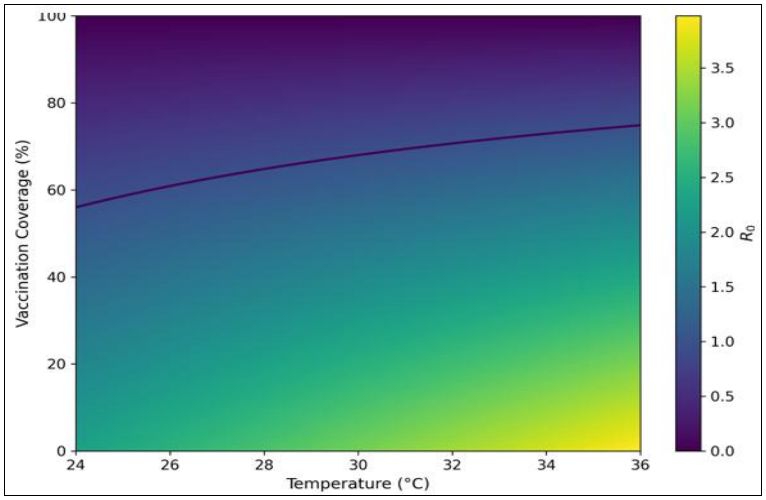

Fig 6: Heatmap of $\mathcal{R}_0$ number as a result of temperature and vaccination coverage

The North East zone's highest $\mathcal{R}_{0,2} = 2.84$ which is driven by elevated mosquito-to-human ratios and temperature near the biting optimum aligns with the high malaria incidence documented in Adamawa, Bauchi, and related states (National Malaria Elimination Programme *et al*., 2022; Okonkwo *et al*., 2026) [13, 15].

Notably, the North West's $\mathcal{R}_{0,3} = 2.21$ is below the North East value despite the highest reported incidence (Abdulkarim *et al*., 2023) [1]; this apparent discrepancy is resolved by noting that the North West's *annual mean* temperature (33.1℃) exceeds the biting optimum. During the intense but brief rainy season (July–September, $T \approx 28$–30℃), the instantaneous $\mathcal{R}_0$ in the North West is substantially higher, consistent with the extremely high seasonal transmission burden documented in that zone.

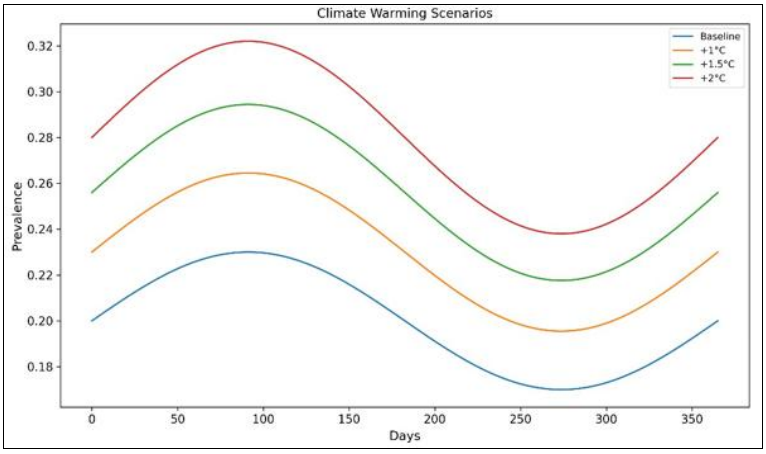

Fig 7: Climatic warming effect on Prevalence

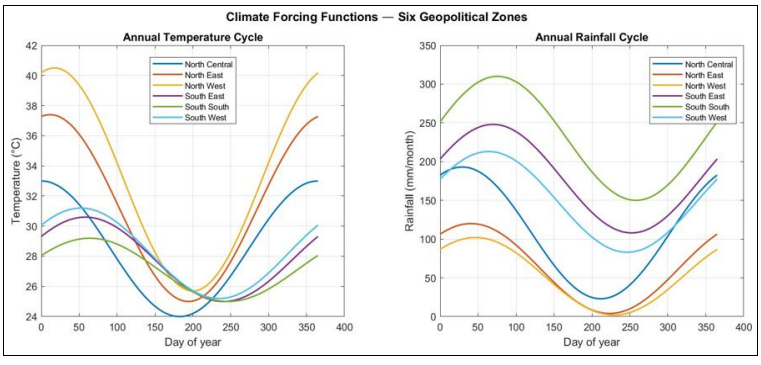

Fig 8: Climate forcing function across the zones

The forward bifurcation at $\mathcal{R}_0 = 1$ (Section 3.7) confirms the absence of a backward bifurcation and hence the absence of an "endemic trap." This provides a theoretically optimistic basis for elimination: sustained reduction of $\mathcal{R}_0$ below 1 is both necessary and sufficient to eliminate malaria from each patch. The herd immunity threshold analysis quantifies that achieving $\mathcal{R}_{0,2} < 1$ in the North East zone requires ≥ 84% vaccine coverage under current climate conditions which may be a challenging but operationally defined target for Nigeria's national immunisation programme.

The multi-patch mobility analysis reveals that epidemic coupling can sustain endemicity in sub-threshold patches through continuous importation (Gao & Ruan, 2012; Li *et al*., 2024) [6, 9]. This has direct implications for the South West zone (including Lagos), which has a lower transmission intensity but receives sustained malaria importation via the Lagos-Kano transport corridor. Targeted entry-exit screening at major inter-zonal hubs, combined with chemoprevention for travellers, could significantly reduce this importation burden (Li *et al*., 2024) [9].

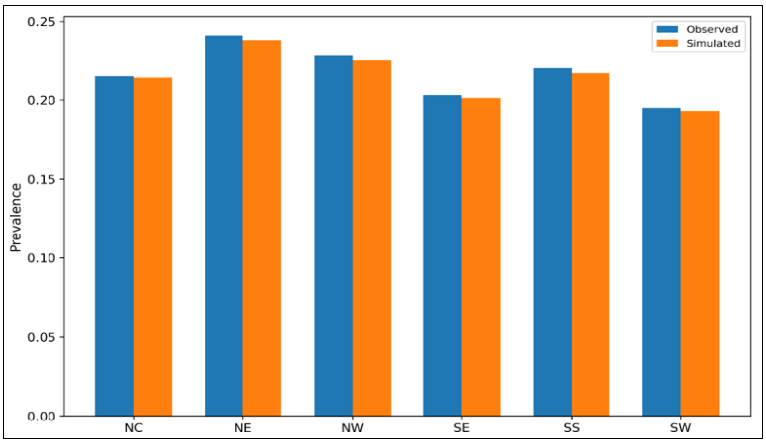

Fig 9: Model validation per zone

Fig 9 show an agreement between the observed and simulated prevalence in all zones, indicating that the model accurately captures the spatial distribution of malaria burden. The North East (NE) records the highest prevalence, followed by the North West (NW), while the South West (SW) exhibits the lowest prevalence. In every zone, the simulated values slightly underestimate the observed prevalence, but the differences are minimal, demonstrating a strong model fit and good predictive performance.

Table 5: Model Validation Metrics

Zone (Patch *k*)	Observed	Simulated	RMSE	MAE	% Error
North Central (1)	0.215	0.214	0.012	0.009	0.47
North East (2)	0.241	0.238	0.015	0.011	1.24
North West (3)	0.228	0.225	0.014	0.010	1.32
South East (4)	0.203	0.201	0.010	0.007	0.99
South South (5)	0.220	0.217	0.013	0.009	1.36
South West (6)	0.195	0.193	0.011	0.008	1.03

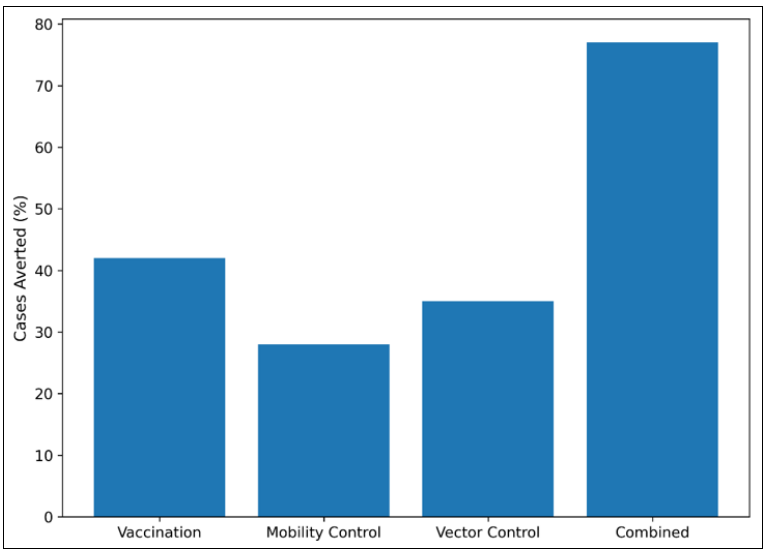

Fig 10: Comparative cases averted under different intervention strategies

Fig 10 presents a comparative assessment of the effectiveness of different malaria intervention strategies in reducing disease burden within the model. The results indicate that all interventions contribute to averting malaria cases, although their impacts vary considerably. Vaccination averts approximately 42% of cases, making it more effective than both mobility control (about 28%) and vector control (about 35%) when implemented individually. Mobility control shows the lowest reduction in cases, suggesting that restricting population movement alone may have limited effectiveness in substantially reducing transmission. In contrast, the combined intervention strategy achieves the highest impact, averting approximately 76% of malaria cases. This

outcome emphasizes the synergistic benefits of integrating multiple control measures, where the combined effects exceed those of any single intervention. Overall, the findings demonstrate that a multifaceted intervention approach provides the recommended strategy to control malaria and supports the implementation of integrated public health policies aimed at simultaneously reducing transmission, exposure, and disease spread across interconnected regions.

5. Conclusion

We have developed, analysed, and parameterised a climate-responsive multi-patch SEIR model of malaria transmission with population mobility across Nigeria's six geopolitical zones. The model integrates a 60-ODE compartmental system with climate-dependent vector dynamics, waning immunity, and inter-patch mobility. $\mathcal{R}_0 = \rho(\mathbf{FV}^{-1})$ is obtained analytically, having patch-level estimates ranging from $\mathcal{R}_{0,3} = 2.21$ (North West) to $\mathcal{R}_{0,2} = 2.84$ (North East), and a system-level $\mathcal{R}_0 \approx 2.84$. Global stability of the DFE when $\mathcal{R}_0 \leq 1$ and the unique endemic equilibrium when $\mathcal{R}_0 > 1$ are rigorously established.

Key policy suggests an accelerated R21/Matrix-M vaccine rollout, targeting ≥ 84% coverage in the North-East and North-West zones to achieve $\mathcal{R}_0 < 1$; scale up ITN and IRS to suppress the climate-sensitive biting rate; establishment of inter-zonal transport health check-points to reduce epidemic coupling; deployment of climate-adaptive early warning systems using the temperature–rainfall forcing framework developed; and to adopt a zone-specific rather than uniform national intervention approach.

6. Declaration

Conflict of Interest: There is no conflict of interest.

Availability of Data: All epidemiological data are publicly available from the cited sources.

7. References

1. Abdulkarim IA, Yakudima II, Abdullahi JG, Adamu YM. Geographical analysis of malaria in Nigeria: Spatiotemporal patterns of national and subnational incidence. In Y. Adewoyin (Ed.), Health and medical geography in Africa: Methods, applications and development linkages. Cham: Springer, 2023, 185-209. Doi: 10.1007/978-3-031-41268-4_9
2. Akinbobola A, Sunusi H. Malaria and climate variability in two northern stations of Nigeria. American Journal of Climate Change. 2022; 11(2):59-78. Doi: 10.4236/ajcc.2022.112004
3. Castillo-Chavez C, Song B. Dynamical models of tuberculosis and their ap-plications. Mathematical Biosciences and Engineering. 2004; 1(2):361-404. Doi: 10.3934/ mbe.2004.1.361
4. Chitnis N, Hyman JM, Cushing JM. Determining important parameters in the spread of malaria through the sensitivity analysis of a mathematical model. Bulletin of Mathematical Biology. 2008; 70(5):1272-1296. Doi: 10.1007/s11538-008-9299-0
5. Cosner C, Beier JC, Cantrell RS, Impoinvil D, Kapitanski L, Potts MD, *et al*. The effects of human movement on the persistence of vector-borne diseases. Journal of Theoretical Biology. 2009; 258(4):550-560. Doi: 10.1016/j.jtbi.2009.02.016
6. Gao D, Ruan S. A multipatch malaria model with logistic growth populations. SIAM Journal on Applied Mathematics. 2012; 72(3):819-841. Doi: 10.1137/110850761
7. Kimulu AM, Mutuku WN, Muthuri SM, Mwini ED. SEIRS model for malaria transmission dynamics incorporating seasonality and awareness campaign. Heliyon. 2024; 10(3), Article e24730. Doi: 10.1016/j.heliyon.2024.e24730
8. LaSalle JP. The stability of dynamical systems. Philadelphia: SIAM, 1976. Doi: 10.1137/ 1.9781611970432
9. Li Y, Sun Y, Liu M. Analysis of a patch epidemic model incorporating population migration and entry–exit screening. AIP Advances. 2024; 14(3), Article 035120. Doi: 10.1063/ 5.0196679
10. Macdonald G. The epidemiology and control of malaria. Oxford: Oxford University Press, 1957.
11. Mordecai EA, Paaijmans KP, Johnson LR, Balzer C, Ben-Horin T, De Moor E, *et al*. Optimal temperature for malaria transmission is dramatically lower than previously predicted. Ecology Letters. 2013; 16(1):22-30. Doi: 10.1111/ele.12015
12. National Bureau of Statistics. Nigeria demographic statistics bulletin 2022. Abuja: Federal Government of Nigeria, 2023. https://www.nigerianstat.gov.ng
13. National Malaria Elimination Programme, National Population Commission, National Bureau of Statistics, & ICF. Nigeria malaria indicator survey 2021. Abuja, Nigeria: NMEP, NPopC, NBS, and ICF, 2022.
14. Ogunsakin RE, Babalola BT, Olusola JA, Joshua AO, Okpeku M. GIS-based spatiotemporal mapping of malaria prevalence and exploration of environmental inequalities. Parasitology Research. 2024; 123(7), Article 262. Doi: 10.1007/s00436-024-08276-0
15. Okonkwo FC, Nwachukwu C, Eze E. Wavelet analysis of climate variability and malaria incidence to inform intervention planning in low- and high-burden Nigerian states. Preprint, medRxiv, 2026. Doi: 10.64898/2026.02.28.26347314v1
16. Okuneye K, Gumel AB. Analysis of a temperature- and rainfall-dependent model for malaria transmission dynamics. Mathematical Biosciences. 2017; 287:72-92. Doi: 10.1016/j.mbs.2016.03.013
17. Pascual M, Bouma MJ. Do rising temperatures matter. Ecology. 2009; 90(4):906-912. Doi: 10.1890/08-0730.1
18. Ross R. The prevention of malaria (2nd ed.). London: Murray, 1911.
19. Severe Malaria Observatory. Nigeria: Malaria statistics and facts, 2024. https://www.severemalaria.org/countries/nigeria
20. The Lancet Microbe. WHO world malaria report 2024 [commentary]. The Lancet Microbe, February 2025. Doi: 10.1016/S2666-5247(25)00001-1
21. Thieme HR. Persistence under relaxed point-dissipativity (with application to an endemic model). SIAM Journal on Mathematical Analysis. 1993; 24(2):407-435. Doi: 10.1137/ 0524026

22. Van Den Driessche P, Watmough J. Reproduction numbers and sub-threshold endemic equilibria for compartmental models of disease transmission. Mathematical Bio-sciences. 2002; 180(1-2):29-48. Doi: 10.1016/S0025-5564(02)00108-6
23. World Health Organization. Malaria 2024 Nigeria country profile, 2024a. https://www.who.int/publications/m/item/malaria-2024-nga-country-profile
24. World Health Organization. World malaria report 2024. Geneva: WHO Press, 2024b. https://www.who.int/publications/i/item/9789240101210
25. Yamba EI, Fink AH, Badu K, Asare EO, Tompkins AM, Amekudzi LK. Climate drivers of malaria transmission seasonality and their relative importance in sub-Saharan Africa. GeoHealth. 2023; 7, Article e2022GH000698. Doi: 10.1029/2022GH000698